CK2-regulated schwannomin-interacting protein IQCJ-SCHIP-1 association with AnkG contributes to the maintenance of the axon initial segment

Marie-Jeanne Papandréou, Helene Vacher, Marie-Pierre Fache, Esther Klingler, Fanny Rueda-Boroni, Géraldine Ferracci, Claire Debarnot, Christelle Piperoglou, Gontzal Garcia del Caño, Laurence Goutebroze, et al.

HAL Id: hal-01701428
https://hal.science/hal-01701428

Submitted on 13 Jul 2018

CK2-regulated schwannomin-interacting protein IQCJ-SCHIP-1 association with AnkG contributes to the maintenance of the axon initial segment

Marie-Jeanne Papandréou,* Hélène Vacher,* Marie-Pierre Fache,* Esther Klingler,† Fanny Rueda-Boroni,* Géraldine Ferracci,* Claire Debarnot,* Christelle Pipéroglou,* Gontzal Garcia Del Caño,*,‡ Laurence Goutebroze† and Bénédicte Dargent*

*CRN2M-UMR7286, Aix Marseille Université, CNRS, Marseille, France
†Institut du Fer à Moulin, Inserm, UMR-S 839, Université Pierre et Marie-Curie, Paris, France
‡Department of Neurosciences, University of the Basque Country, Vitoria-Gasteiz, Spain

Abstract

The axon initial segment (AIS) plays a central role in electrogenesis and in the maintenance of neuronal polarity. Its molecular organization is dependent on the scaffolding protein ankyrin (Ank) G and is regulated by kinases. For example, the phosphorylation of voltage-gated sodium channels by the protein kinase CK2 regulates their interaction with AnkG and, consequently, their accumulation at the AIS. We previously showed that IQ motif containing J-Schwannomin-Interacting Protein 1 (IQCJ-SCHIP-1), an isoform of the SCHIP-1, accumulated at the AIS in vivo. Here, we analyzed the molecular mechanisms involved in IQCJ-SCHIP-1-specific axonal location. We showed that IQCJ-SCHIP-1 accumulation in the AIS of cultured hippocampal neurons depended on AnkG expression. Pull-down assays and surface plasmon resonance analysis demonstrated that AnkG binds to CK2-phosphorylated IQCJ-SCHIP-1 but not to the non-phosphorylated protein. Surface plasmon resonance approaches using IQCJ-SCHIP-1, SCHIP-1a, another SCHIP-1 isoform, and their C-terminus tail mutants revealed that a segment including multiple CK2-phosphorylatable sites was directly involved in the interaction with AnkG. Pharmacological inhibition of CK2 diminished both IQCJ-SCHIP-1 and AnkG accumulation in the AIS. Silencing SCHIP-1 expression reduced AnkG cluster at the AIS. Finally, over-expression of IQCJ-SCHIP-1 decreased AnkG concentration at the AIS, whereas a mutant deleted of the CK2-regulated AnkG interaction site did not. Our study reveals that CK2-regulated IQJC-SCHIP-1 association with AnkG contributes to AIS maintenance.

Keywords: ankyrin G, axon initial segment, protein kinase CK2, SCHIP-1.

J. Neurochem. (2015) **134**, 527–537.

The axon initial segment (AIS) is a highly specialized axonal region that plays a key role in the physiology of mammalian neurons. The AIS not only contains high densities of voltage-gated sodium (Na_v) and potassium (K_v) channels responsible for the action potential firing, but it is also critical for the maintenance of the axonal identity (Leterrier and Dargent 2014). These roles are sustained by the unique molecular architecture of the AIS, which is driven by the scaffolding protein, ankyrin (Ank) G. AnkG is the earliest protein to be targeted to the AIS where it interacts with the actin cytoskeleton *via* βIV-spectrin (Komada 2002) and with microtubules through EB1/3 proteins (Leterrier *et al.* 2011). AnkG also associates with $Na_v1.1$, $Na_v1.2$ and $Na_v1.6$, and KCNQ2/3

channels and concentrates them to the AIS (Garrido 2003; Lemaillet 2003; Pan 2006). AnkG binds to the membrane protein neurofascin 186 (Nf-186) that interacts with extracellular matrix proteins (Hedstrom *et al.* 2007). The crucial role of AnkG in orchestrating the AIS assembly and maintenance was demonstrated by *in vivo* or *in vitro* depletion of AnkG. Both depletions prevented AIS formation or dismantled the mature AIS and caused axons to acquire the molecular characteristics of dendrites (Jenkins 2001; Hedstrom *et al.* 2007, 2008; Sobotzik *et al.* 2009). During development, AnkB together with αII- and βII-spectrin form an intra–axonal boundary limiting AnkG incorporation into the distal axonal submembranous cytoskeleton and eventually causes its accumulation at the proximal axon (Galiano *et al.* 2012).

We previously showed that IQ motif containing J-Schwannomin-Interacting Protein 1 (IQCJ-SCHIP-1), an isoform of SCHIP-1, is also highly enriched at the AIS *in vivo* (Martin *et al.* 2008). Its accumulation at the AIS depends on the presence of AnkG and βIV spectrin (Martin *et al.* 2008) but the functional role of IQCJ-SCHIP-1 is still unravelled. Six isoforms produced by alternative splicing of the *Schip1* gene are expressed in mouse brain (SCHIP-1a, SCHIP-1b, and IQCJ-SCHIP-1 (Goutebroze *et al.* 2000; Kwaśnicka-Crawford *et al.* 2006); SCHIP-1c, SCHIP-1d, and IQCJs-SCHIP-1, GenBank accession numbers KM233716, KM233715 and KJ941154). SCHIP-1a and SCHIP-1b were firstly identified by yeast two-hybrid screen as binding partners of schwannomin (Goutebroze *et al.* 2000). IQCJ-SCHIP-1 was originally described as a brain protein potentially involved in language disorder in human (Kwaśnicka-Crawford *et al.* 2006). All SCHIP-1 isoforms share a C-terminal sequence of 234 amino acid residues that contains a leucine zipper coiled–coil domain implicated in their dimerization (Goutebroze *et al.* 2000). The N-terminal part of IQCJ-SCHIP-1 possesses an IQ motif and associates with calmodulin in the absence of Ca++(Bähler and Rhoads 2002; Martin *et al.* 2008). This motif is present in IQCJ-SCHIP-1 isoform but absent from the others isoforms. The coiled–coil domain of SCHIP-1 presents about 70% of conserved residues with one of the four coiled–coil domains of fasciculation and elongation proteins zeta and their *Caenorhabditis elegans* ortholog (Goutebroze *et al.* 2000). Fasciculation and elongation proteins zeta proteins are involved in vesicular transport in axons in association with the motor protein kinesin 1 (Bloom and Horvitz 1997; Gindhart *et al.* 2003; Blasius *et al.* 2007; Fujita *et al.* 2007; Ikuta *et al.* 2007). Moreover, the C-terminal part of SCHIP-1 proteins contains a domain of about 50 amino acids, including 12 serines and threonines phosphorylatable by CK2 (Fig. 2a) (CK2-phosphorylation sites predicted, using GPS 2.0 application, Xue *et al.* 2008). Interestingly, protein kinase CK2 was found to be enriched at the AIS *in vivo* and in cultured hippocampal neurons, where it phosphorylated key serine residues of the ankyrin-binding motif of $Na_v1.2$ and $Na_v1.6$ channels, influencing both AnkG and Na_v accumulation at the

AIS and neuronal excitability (Brechet *et al.* 2008; Brachet *et al.* 2010; Gasser *et al.* 2012; Hien *et al.* 2014).

In this study, we examined whether CK2 and AnkG are involved in the accumulation of IQCJ-SCHIP-1 at the AIS. We demonstrated that CK2-phosphorylation regulated IQCJ-SCHIP-1 association with AnkG. The comparison of AnkG-binding properties of IQCJ-SCHIP-1, SCHIP-1a and of their C-terminal tail mutants showed that CK2-phosphorylation domain was directly involved in the interaction with AnkG. Pharmacological inhibition of CK2 diminished both IQCJ-SCHIP-1 and AnkG accumulation in the AIS. Silencing SCHIP-1 expression reduced AnkG clustering at the AIS. Finally, over-expression of IQCJ-SCHIP-1 decreased AnkG concentration at the AIS, whereas a mutant deleted of the CK2-regulated AnkG interaction site did not. Our study reveals that CK2-regulated IQJC-SCHIP-1 association with AnkG contributes to AIS maintenance.

Experimental procedures

Animals

All procedures were in agreement with the European Communities Council directive (86/609/EEC). Experiments were performed on pregnant females Wistar rat or Swiss mice (Janvier labs, Laval, France). Animals were sacrificed by decapitation and embryo brains were used for primary neuronal cell culture.

Plasmids, recombinant protein expression and purification

DNA containing sequence for shRNA against AnkG (Hedstrom *et al.* 2007) or Firefly luciferase (SHC007; Sigma-Aldrich, Saint-Louis, MO, USA) together with a nine nucleotides loop region (TTCAAGAGA) and flanked by H1 and U6 promoters were chemically synthesized and inserted into pCR^{R}2.1-TOPO (Eurofins MWG/operon, Eberberg, Germany). DNA containing sequence for shRNA against SCHIP-1 (5′-TGCCTCACATAAGCGAATGTT-3′) together with a nine nucleotides loop region (TTCAAGAGA) and flanked by nucleotides for *Bbs*I restriction sites was chemically synthesized and subcloned into the double-promoter pFIV-H1/U6 siRNA cloning vector (System Biosciences, Ebersberg, Germany). The efficiency of the resulting vector was verified by performing western blot on lysates from COS-7 cells cotransfected with an expressing vector for Flag-tagged IQCJ-SCHIP-1 (vector pFLAG-CMV-2; Sigma-Aldrich) (data not shown). shRNA expression cassettes were then subcloned into *Eco*R1/*Bst*BI of the modified pFUGW vector (Lois 2002) where the EGFP was replaced by farnesylated enhanced green fluorescent protein (EGFP) (from pEGFP-F; Clontech, Rockville, MD, USA). The human nucleotide sequence of SCHIP-1a was amplified by PCR (Expand High Fidelity Taq Polymerase; Roche Molecular Biochemicals, Indianapolis, IN, USA) on pEGFPC3-SCHIP-1a. PCR products were inserted into pCRII-TOPO (TOPO TA Cloning; Life Technologies, Grand Island, NY, USA) and subcloned by restriction into pGEX-6P1 (GE Healthcare, Life Science, Little Chalfont, UK). The resulting plasmid (pGEX-SCHIP-1a) drives the expression of GST-SCHIP-1a. To generate the truncated GST-SCHIP-1a mutants, desired restriction sites were introduced on pGEX-SCHIP-1a using Quick Change XL site mutagenesis kit (Stratagene, La Jolla, CA,

USA). Plasmids expressing mutants were further obtained by enzymatic deletion of the desired region on modified pGEX-SCHIP-1a vector. Human nucleotide sequence specific for IQCJ-SCHIP-1 (aa 1–92) flanked by restriction sites was chemically synthesized and inserted into pCR^{R}2.1-TOPO (Eurofin MWG/operon). This sequence was sub-cloned by restriction in the modified pGEX-SCHIP-1a to produce pGEX-IQCJ-SCHIP-1. The pFlag-CMV2 IQCJ-SCHIP-1 (Flag-IQCJ-SCHIP-1) was obtained by PCR amplification of the IQCJ-SCHIP-1 cDNA and subcloning into NotI/Bg/II sites of pFlag-CMV2 vector. The C-terminal tail mutant deleted of its 180 last amino acids (Flag-IQCJ-SCHIP-1-Δter) was generated by subcloning into NotI/EcoRV sites of the pFlag-CMV2 vector. All constructs were verified by DNA sequencing (Beckman Coulter Genomics, Danvers, MA, USA). Plasmid expressing GST-Na$_v$1.2$_{1080-1203}$ was described in (Brechet et al. 2008). Plasmid expressing rat 270 kDa-AnkG-GFP (Green Fluorescent Protein), purified histidine-tagged human 220 kDa-AnkB and purified rat 190 kDa-AnkG (Zhang and Bennett 1998) were kindly provided by Dr V. Bennett, (Duke University, Durham, NC, USA). All GST-constructs were expressed in BL21 Escherichia Coli. Transformed bacteria were grown in M9 minimum medium, supplemented with 3% ethanol during IPTG induction. GST fusion proteins were purified by chromatography on gluthatione-Sepharose 4B according to the manufacturer's instructions (GE Healthcare). Protein concentrations were determined by the bicinchoninic acid method (Thermo Fisher Scientific, Waltham, MA, USA).

GST pull–downs

COS-1 cells were transfected with 270 kDa-AnkG-GFP plasmid using Lipofectamine 2000, according to the manufacturer's instructions (Invitrogen, Carlsbad, CA, USA). Transfected cells were solubilized in Tris-buffered saline (10 mM Tris, pH 7.5, 150 mM NaCl) containing 1 mM EDTA, 1% Triton X-100, 0.1% deoxycholate, and protease inhibitors (complete EDTA-free; Roche Molecular Biochemicals) for 45 min at 4°C. Insoluble proteins were removed by centrifugation at 14 000 g for 15 min at 4°C. GST-proteins (1 μM in 200 μL of kinase buffer supplied by the manufacturer) were phosphorylated as previously described in (Brechet et al. 2008) with 200 μM ATP (Invitrogen) and 1000 U of CK2 (New England Biolabs, Inc) for 30 min at 30°C. To study the interaction with AnkG, GST-proteins were further incubated with 1 mL of COS-1 cell lysate for 4 h at 4°C. Glutathione Sepharose 4B (40 μL) was then added for 1 additional hour. Alternatively, to test SCHIP-1 interaction with calmodulin, GST-proteins were first incubated with Glutathione Sepharose 4B (40 μL) for 1 h. Beads were washed four times and were resuspended in Tris-buffered saline supplemented with CaCl$_2$ (2 mM) or EGTA (2 mM). Purified calmodulin from bovine brain (Calbiochem, San Diego, CA, USA) (2 μM in 250 μL) was further added to GST-fusion proteins for 2 additional hours. After extensive washes, pull-down samples were resolved by sodium dodecyl sulfate–polyacrylamide gel electrophoresis and immunoprobed with anti-GST (1/250; Abcam, Cambridge, UK) or anti-calmodulin (1/1000; 05-173; Upstate Biotechnology, Lake Placid, NY, USA) antibodies (Abs).

Surface plasmon resonance

Surface plasmon resonance (SPR) experiments were performed at 25°C on a Biacore 3000 instrument with CM5 sensor chip, using HBS-EP running buffer (GE Healthcare) as previously described (Brechet

et al. 2008). Briefly, GST or GST-SCHIP-1 proteins were immobilized in flow cells via a polyclonal anti-GST Ab. When indicated, CK2-phosphorylation was directly performed onto the chip according to (Catimel et al. 2006). Purified 190 kDa-AnkG and 220 kDa-AnkB were serially diluted two fold in running buffer from 0.5 to 800 nM. Samples were injected sequentially at 20 μL/min using the single-cycle kinetic method with an association time of 180 s and a dissociation time of 60 s, except for the last injection, in which the dissociation time was extended to 15 min (Karlsson et al. 2006). The non-specific signal (GST) was subtracted from the total signal (GST fusion protein) and control-run injections of buffer were performed in the same conditions before Ank injections and subtracted for data analysis. Binding parameters were measured by globally fitting sensorgrams with the 1 : 1 titration kinetic-binding model with BIAcore evaluation software version 4.1(Palau and Di Primo 2013).

Cell culture, transfection, pharmacological treatment immunofluorescence, and western blot analysis

Primary hippocampal neurons were prepared as described previously (Garrido 2003). Amaxa mice neuron nucleofactor kit (Lonza, Basel, Switzerland) was used to nucleofected dissociated mouse neurons with shRNA against SCHIP-1a or shRNA against luciferase or dissociated rat neurons with shRNA against AnkG or shRNA against luciferase. Mouse neurons were processed for immunofluorescences 7 days after transfection and rat neurons were immunostained 10 days post-tranfection, when all neurons were positive for both AnkG and SCHIP-1 staining. Alternatively, 7 days in vitro (DIV) rat neurons were transfected with Flag-IQCJ-SCHIP-1 or Flag-IQCJ-SCHIP-1-ΔCter, using Lipofectamine 2000 (Invitrogen) according to the manufacturer's instructions. Neurons were processed for immunofluorescence 3 days post-transfection. Inhibition of CK2 activity was performed on 9–10 DIV rat neurons, using 4,5,6,7-tetrabromobenzotriazole (TBB, Biaffin GmbH and CoKG: 5 μM in 0.05% dimethylsulfoxide). Controls included the same amount of dimethylsulfoxide. For immunostaining, neurons were blocked for non-specific binding for 30 min in blocking buffer (0.22% gelatin, 0.066% saponin in 0.1 M phosphate buffer) after fixation in methanol (7 min, −20°C). Proteins were probed with anti-SCHIP (1/100; 17141 directed against the sequence 112-305 of SCHIP-1a, 15013 directed against the sequence 1-97 of IQCJ-SCHIP-1, Martin et al. 2008), anti-AnkG (1/400; N106/65 and N106/36; from UC Davis/NIH NeuroMab Facility), anti-microtubule-associated protein 2 (MAP2, 1/2000; ab5392; Abcam), anti-CK2 (1/50; sc6479; Santa Cruz Biotechnology, Santa Cruz, CA, USA), anti-Nf-186 (1/300; A12/18; NeuroMab), and anti-GFP (1/5000, ab 290; Abcam) Abs for 1 h. Corresponding secondary Abs conjugated to Alexa 488, 555, 633 (Invitrogen) or to Dylight 405 (Rockland, Limerick, PA, USA) were incubated for 1 h. Coverslips were mounted in FluorSave reagent (Calbiochem). For western blot analysis, rat neurons cultured from 7 to 21 DIV were solubilized in 10 mM phosphate buffer pH 7.4, 150 mM NaCl, 0.3% sodium dodecyl sulfate. Protein levels were normalized against β-tubulin before western blot analysis. Anti-SCHIP-1 Abs (1 : 200) and anti-β-tubulin Ab (1/1000, clone E7; Developmental Studies Hybridoma Bank, University of Iowa, Iowa, USA) were used for immunoblots.

Confocal microscopy and quantification

Immunostained neurons were imaged using a Zeiss LMS780 (Zeiss, Jena, Germany) confocal microscope equipped with a

63×1.4 N.A. oil immersion objective. Fluorescence was collected as Z stacks with sequential wavelength acquisition. Quantification was performed using NIH imageJ software (National Institute of Health, Bethesda, MD, USA). To determine the effect of shRNAs expression, protein immunostaining intensity in the AIS was measured in transfected and in surrounding non-tranfected cells and was expressed as an AIS intensity ratio. Similar measurements were done to examine the impact of IQCJ-SCHIP-1 over-expression. The axonal polarity index i.e., the ratio of average fluorescent intensity for the AIS to dendrite branches, was used to determine the effect of TBB treatments on the localization of AIS proteins. Regions of interest corresponding to AIS were manually selected on AnkG images and reported on other channels for intensity measurements. All intensities were corrected for background labelling. For illustration, image editing was performed using ImageJ or Photoshop 7.0 software (Adobe) and was limited to rolling-ball background subtraction, linear contrast enhancement, and gamma adjustment.

Statistical analysis

Results are expressed as mean $\pm$ SEM. Statistical analysis was performed using PRISM 5 (Graphpad software, La Jolla, CA, USA). Significance of the differences was assessed using a two-tailed *t*-test: ***$p < 0.0001$.

Results

Effect of AnkG silencing on IQCJ–SCHIP–1 accumulation at the AIS of hippocampal neurons

We used two anti-SCHIP-1 antibodies (Abs) characterized previously (Martin *et al.* 2008) to evaluate the expression of SCHIP-1 in hippocampal neurons maintained in culture. The 17141 Ab recognized an epitope present only in SCHIP-1a and in IQCJ-SCHIP-1 and did not show any reactivity for the shorter form, SCHIP-1b (Martin *et al.* 2008). The 15013 Ab was directed against the first 97 amino acids of IQCJ-SCHIP-1, which are specific to this isoform (Fig. 2a). We performed western blot analyses on lysates of neurons collected at different days of culture. Western blotting with either 17141 or 15013 Abs revealed a single protein with an apparent molecular weight of about 65 kDa (Fig. 1a and b), corresponding to IQCJ-SCHIP-1. Accordingly, the AIS of 10 DIV neurons, identified by AnkG labeling, were positive for SCHIP-1 staining by both anti-SCHIP-1 Abs (Fig. 1c and d). AnkG knockdown has been shown to perturb the location of all tested AIS constituents (e.g., Nf-186, Na_v1 channels and βIV-spectrin) and to affect proximal axon molecular identity (Hedstrom *et al.* 2008). Thus, we next evaluated the effect of AnkG depletion on IQCJ-SCHIP-1 accumulation at the AIS. Cultured hippocampal neurons were transfected with farnesylated-GFP shRNA against AnkG (shAnkG) or against luciferase (shcontrol), used as a control (Fig. 1e–g). AnkG immunofluorescent intensity was strongly reduced in shAnkG-transfected neurons as compared to what was observed in shcontrol neurons (ratio of AIS intensity in the transfected neuron to that in the surrounding non-transfected cells,

0.33 ± 0.03 for shAnkG ($n = 19$), 0.93 ± 0.07 for shcontrol ($n = 16$); 2 independent experiments). This was accompanied by a decrease in IQCJ-SCHIP-1 concentration in the AIS (ratio of AIS intensity 0.31 ± 0.04 for shAnkG, 0.92 ± 0.08 for shcontrol). We concluded that AnkG is necessary for the recruitment and/or for the retention of IQJC-SCHIP-1 to the AIS.

Protein kinase CK2–phosphorylation regulated IQCJ–SCHIP–1 binding to AnkG

To characterize the molecular mechanisms by which IQCJ-SCHIP-1 concentrates at the AIS, we next subjected cell lysates from COS-1 cells expressing 270 kDa-AnkG-GFP to GST pull-down assays with IQCJ-SCHIP-1 or with the canonical SCHIP-1a. As shown in Fig. 2(b) and (c), neither GST-IQCJ-SCHIP-1 nor GST-SCHIP-1a were able to bind to AnkG, unlike GST-$Na_v1.2_{1080\text{-}1203}$ used as a positive control. We previously demonstrated that the phosphorylation of GST-$Na_v1.2_{1080\text{-}1203}$ by CK2 greatly enhanced its interaction with AnkG (Brechet *et al.* 2008). Since both SCHIP-1 proteins possess a domain predicted as phosphorylatable by this kinase (Fig 2a), we examined if CK2-phosphorylation of SCHIP-1 was necessary for its interaction with AnkG. As expected (Brechet *et al.* 2008; Hien *et al.* 2014), the binding of AnkG-GFP to GST-$Na_v1.2_{1080\text{-}1203}$ was greatly enhanced upon CK2-phosphorylation (Fig. 2b). Both GST-IQCJ-SCHIP-1 and GST-SCHIP-1a were able to interact with AnkG-GFP after their phosphorylation by CK2 (Fig. 2b and c). In parallel, we wondered whether CK2-phosphorylation could also impact IQCJ-SCHIP-1 binding to calmodulin. We tested the ability of GST-IQCJ-SCHIP-1 phosphorylated or not by CK2, to associate with purified calmodulin in the presence of either $CaCl_2$ or EGTA. GST-SCHIP-1a was used as a negative control. We observed that calmodulin associated with both phosphorylated and non-phosphorylated forms of IQCJ-SCHIP-1 in the absence of Ca^{2+} (Fig. 2d). Altogether, these results demonstrated that CK2-phosphorylation regulates IQCJ-SCHIP-1 binding to AnkG but not calmodulin association. Moreover, these data suggested that the N-terminal part of the IQCJ-SCHIP-1 that contains the IQ motif, is not required for AnkG binding.

The phosphorylation domain of SCHIP–1 was involved in the binding to AnkG

We next used SPR technology to quantitatively analyze the interaction between AnkG and IQCJ-SCHIP-1 i.e., to determine the binding properties of IQCJ-SCHIP-1 and its interaction domain to AnkG. GST-IQCJ-SCHIP-1 or GST-SCHIP-1a were purified and immobilized on the sensor surface by immunoaffinity. When sequential increasing concentrations of purified 190 kDa-AnkG were injected over flow cells, no significant reactivity was observed demonstrating that non-phosphorylated GST-SCHIP-1 proteins did not associate with AnkG, in good agreement with
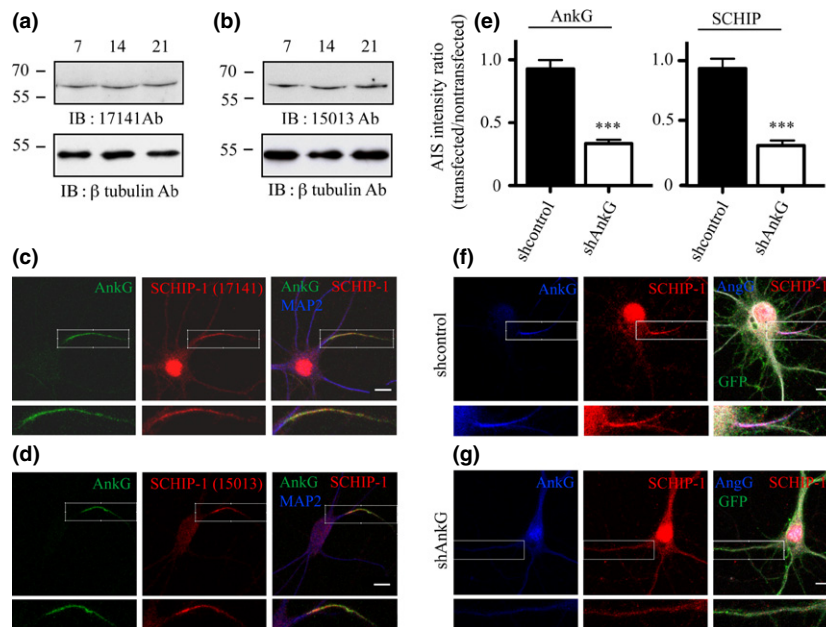
Fig. 1 Effect of ankyrin (Ank) G silencing on IQ motif containing J-Schwannomin-Interacting Protein 1 (IQCJ-SCHIP-1) accumulation at the axon initial segment (AIS). (a and b) Detection of IQCJ-SCHIP-1 expression in cultured hippocampal neurons by western blot. Lysates of neurons cultured from 7 to 21 DIV were analyzed on 12% sodium dodecyl sulfate–polyacrylamide gel electrophoresis (SDS–PAGE) and immunoblotted (IB) with the 17141 (a) or 15013 (b) Abs as indicated (top panels). Lysates were normalized against tubulin expression (bottom panels). (c and d) Detection of IQCJ-SCHIP-1 expression by immunostaining. 10 DIV neurons were stained with 17141 Ab (red, c) or 15013 Ab (red, d) and Abs to AnkG (green) and MAP2 (blue). Scale bars = 10 μm. (e–g) Effect of AnkG silencing on AnkG and IQCJ-SCHIP-1 stainings at the AIS. Neurons transfected with either shluciferase used as a control (f) or shAnkG (g) were stained with 17141 (red), anti-GFP (green) and anti-AnkG (blue) Abs. Scale bars = 10 μm. (e) AIS intensity ratio in the transfected neuron to that in surrounding non-transfected cells for AnkG and IQCJ-SCHIP-1. ***$p < 0.0001$

GST pull-down assays (Fig. 3a, b and Table 1). It was only after CK2-phosphorylation performed on immobilized GST-IQJC-SCHIP-1 and GST-SCHIP-1a, that purified AnkG was able to interact with both proteins with an affinity in the nanomolar range ($K_D = 0.43 \pm 0.19$ nM and $K_D = 0.69 \pm 0.35$ nM, respectively) (Fig. 3a, b and Table 1). AnkB, which possesses about 70% of sequence homology with AnkG, is also highly expressed in axons but presents a distinct location and function from AnkG (Galiano *et al.* 2012). Thus, we wondered if CK2-phosphorylation also regulates SCHIP-1 proteins binding to AnkB. We found that both SCHIP-1 proteins interacted with purified 220 kDa-AnkB, with a nanomolar affinity, solely after their phosphorylation by CK2 (Table 1). We next characterized the AnkG-binding region on SCHIP-1 proteins. Since all SCHIP-1 isoforms differ only in their N-terminal domains, we focused our search on the conserved C-terminal region. We generated three GST fusion proteins fused with (i) the C-terminal moiety of SCHIP-1 (referring as amino acids (aa) 307–487 of SCHIP-1a), (ii) the C-terminus lacking its leucine zipper domain (aa: 307-413), and (iii) the C-terminus lacking the phosphorylation domain (aa: 374-487). Both GST-(307-487) and GST-(307-413) were still able to interact with AnkG after CK2 phosphorylation while GST-(374-487) did not (Fig. 3c and Table 2). These results indicated that the direct interaction between SCHIP-1 proteins and AnkG was mediated through the CK2-phosphorylation domain of SCHIP-1 proteins.

Pharmacological inhibition of CK2 reduced IQCJ–SCHIP–1 and AnkG clustering at the AIS

We tested the impact of the pharmacological inhibition of CK2 on the endogenous IQCJ-SCHIP-1 and AnkG neuronal location. We previously showed that 2-dimethylamino-4,5,6,7-tetrabromo-1H-benzimidazole (DMAT), a CK2 inhibitor, reduced both AnkG and Na_v concentration at the AIS of mature cultured neurons (Brechet *et al.* 2008). DMAT is no longer available; we used instead TBB (Duncan *et al.* 2008). The effect of TBB treatment on the AIS localization of IQCJ-SCHIP-1 and AnkG was analyzed by quantitative immunostaining. The normalized axonal index polarity (API) was determined for AnkG and IQCJ-SCHIP-1 either in TBB-treated cells or in cells treated with the vehicle only (control) (Fig. 4). We observed that TBB treatment (5 μM) reduced both IQJC-SCHIP-1 and AnkG accumulation by about 40% (API = 0.53% ± 0.02 for IQCJ-SCHIP-1
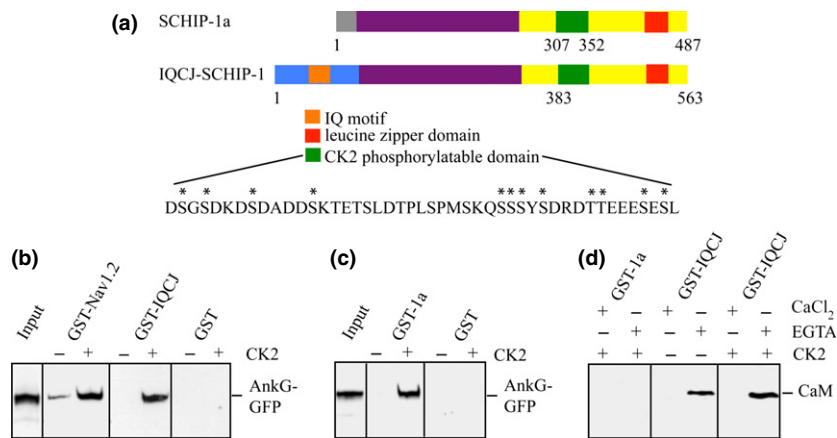
Fig. 2 Effect of CK2 on SCHIP-1 protein association to ankyrin (Ank) G and to calmodulin. (a) Schematic representation of SCHIP-1 isoforms. IQCJ-SCHIP-1 is aligned against SCHIP-1a sequence. Isoforms share a common C-terminal region (yellow box), including a CK2 phosphorylatable domain (green box) and a leucine zipper domain (red box). The N-terminus of SCHIP-1a (gray box) differs with that of IQCJ-SCHIP-1 (blue box), which possesses an IQ motif motif (orange box). The amino-acid sequence of the CK2-phosphorylatable domain is presented; asterisks indicate phosphorylatable Ser and Thr as predicted using GPS 2.0 application (Xue *et al.* 2008). (b and c) Effect of CK2 on SCHIP-1 protein association with AnkG. GST pull-down reactions were performed on 270 kDa-AnkG-GFP (Ank-GFP) lysates using GST-IQCJ-SCHIP-1 (b, GST-IQCJ) and GST-SCHIP-1a (c, GST-1a) *in vitro* phosphorylated or not by CK2. GST-Na$_v$2$_{1080-1203}$ was used as a positive control (b) and GST as a negative one (b and c). AnkG-GFP pulled down was detected by western blot with an anti-GFP Ab. (d) Effect of CK2 on IQCJ-SCHIP-1 association with calmodulin (CAM). Purified CAM pull-downs were performed using either non-phosphorylated GST-IQCJ-SCHIP-1 or CK2-phosphorylated GST-IQCJ-SCHIP-1, in the presence (CaCl$_2$) or absence (EGTA) of Ca^{++}. CK2-phosphorylated GST-SCHIP-1a was used as negative control. CAM pulled down was detected by immunoblotting with an anti-calmodulin Ab.
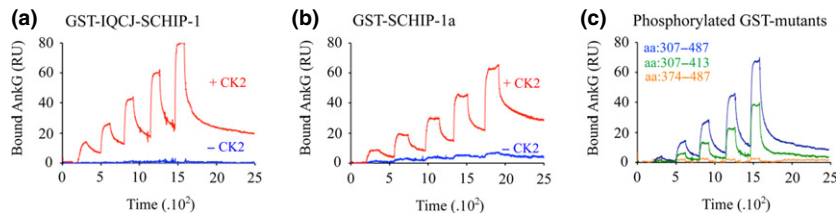
Fig. 3 Analysis of SCHIP-1 protein-binding properties to ankyrin (Ank) B and G. Surface plasmon resonance (SPR) analysis of the direct interaction between SCHIP-1 proteins and AnkG are illustrated by typical sensorgrams. Increasing concentrations of 190 kDa-AnkG were injected on immobilized GST-IQCJ-SCHIP-1 (a), GST-SCHIP-1a (b) before and after *in situ* phosphorylation by CK2 of the immobilized constructs (c). The position of the amino acids was done from the sequence of SCHIP-1a. Only the curves corresponding to the concentrations of AnkG ranging from 0.5 to 8 nM are shown here.

and $0.63\% \pm 0.03$ for AnkG ($n = 115$); 2 independent experiments). Altogether these results demonstrated that the accumulation of IQCJ-SCHIP-1 and AnkG at the AIS depended on CK2 activity.

Depletion of IQCJ–SCHIP–1 expression decreased AnkG clustering in the AIS of hippocampal neurons

Since we previously showed that IQCJ-SCHIP-1 accumulates at the AIS after AnkG (Martin *et al.* 2008) and that AnkG is required for IQCJ-SCHIP-1 clustering at the AIS (Fig. 1e–g), we further examined whether IQCJ-SCHIP-1 expression influences the maintenance of the AIS by testing the impact of IQCJ-SCHIP-1 depletion on AnkG clustering. Cultured hippocampal neurons were transfected with validated farnesylated-GFP shRNA against SCHIP-1 (shS-CHIP-1) or against luciferase (shcontrol). IQCJ-SCHIP-1 intensity was strongly reduced in shSCHIP-1 transfected neurons as compared to what observed in shcontrol neurons (ratio of IQCJ-SCHIP-1 intensity in the transfected neuron to that in surrounding non-transfected cells, 0.66 ± 0.04 for shSCHIP-1 ($n = 60$), 1.04 ± 0.04 for shcontrol ($n = 57$), 3 independent experiments). In neurons

Table 1 Kinetic parameters of the interaction between 190 kDa-AnkG or 220 kDa-AnkB and IQCJ-SCHIP-1 or SCHIP-1a

Immobilized GST-construct	Ank	CK2	k_{on} ($\times 10^6$ M^{-1}s^{-1})	k_{off} ($\times 10^{-3}$ s^{-1})	K_D nM
IQCJ-SCHIP-1	G	−			ND
		+	2.54 ± 0.80	0.98 ± 0.19	0.43 ± 0.19
	B	−			ND
		+	0.66 ± 0.17	0.32 ± 0.09	0.46 ± 0.04
SCHIP-1a	G	−			ND
		+	2.91 ± 3.14	1.51 ± 1.27	0.69 ± 0.35
	B	−			ND
		+	0.58 ± 0.32	0.48 ± 0.34	0.79 ± 0.17

Mean values ± SD are obtained from 2 to 5 experiments. ND, No sufficient specific binding to determine kinetic parameters and K_D.

**Table 2** Kinetic parameters of the interaction between 190 kDa-AnkG and SCHIP-1a mutants

Immobilized GST-SCHIP-1a mutant	CK2	k_{on} ($\times 10^6$ M^{-1}s^{-1})	k_{off} ($\times 10^{-3}$ s^{-1})	K_D nM
aa: 307-487	−			ND
	+	3.80 ± 4.25	1.48 ± 2.64	2.17 ± 2.17
aa: 307-413	−			ND
	+	2.66 ± 2.27	9.3 ± 15.1	2.08 ± 2.68
aa: 374-487	−			ND
	+			ND

Mean values ± SD are obtained from 2 to 5 experiments. ND, No sufficient specific binding to determine kinetic parameters and K_D.

depleted for IQCJ-SCHIP-1, AnkG concentration was also reduced (Fig. 5a–c) (ratio of AIS intensity 0.66 ± 0.03 for shSCHIP-1, 0.99 ± 0.04 for shcontrol). These results indicated that IQCJ-SCHIP-1 influenced AnkG clustering at the AIS.

Over-expression of IQCJ-SCHIP-1 affected AnkG accumulation in the AIS of hippocampal neurons

To further confirm the role of IQCJ-SCHIP-1 on AIS stability, we transfected cultured hippocampal neurons with either Flag-IQCJ-SCHIP-1 or a C-terminal tail mutant lacking the 180 last amino acids (Flag-IQCJ-SCHIP-1-ΔCter). Following 3 days of expression, both Flag-IQCJ-SCHIP-1 and its mutant were expressed throughout the somatodendritic domain identified by MAP2 staining and in axons (Fig. 5d and e). We observed that AnkG clustering was reduced in neurons over-expressing Flag-IQCJ-SCHIP-1, but not in neurons expressing Flag-IQCJ-SCHIP-1-ΔCter, the mutant lacking the CK2-regulated AnkG-binding site (ratio of AIS AnkG intensity in transfected cells versus non-transfected cells, 0.50 ± 0.03 for Flag-IQCJ-SCHIP-1 ($n = 58$) and 0.99 ± 0.04 for Flag-IQCJ-SCHIP-1-ΔCter ($n = 40$); 2 independent experiments (Fig. 5d–f). These results showed that over-expression of IQCJ-SCHIP-1
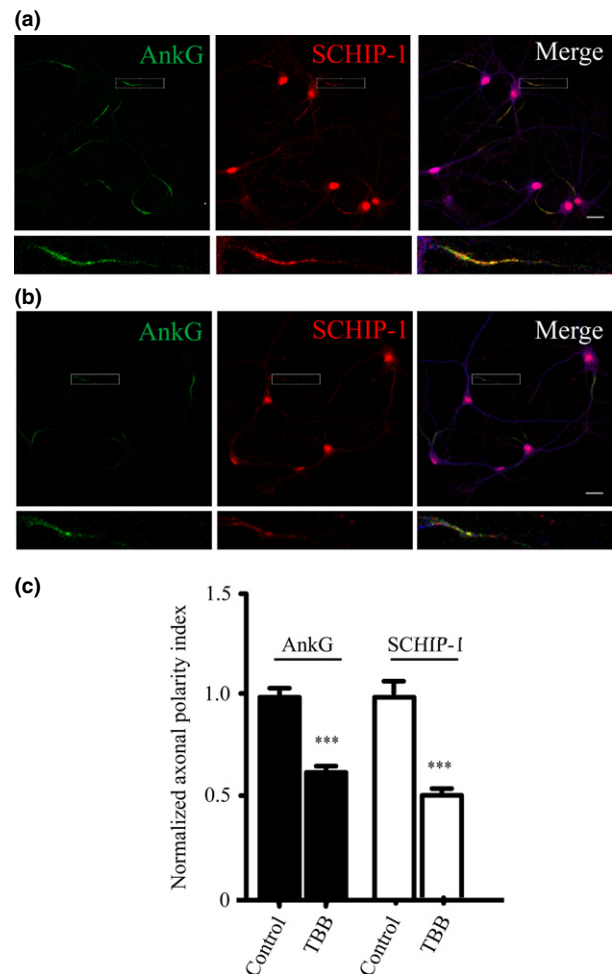
Fig. 4 Effect of CK2 pharmacological inhibition on the axon initial segment (AIS) localization of IQ motif containing J-Schwannomin-Interacting Protein 1 (IQCJ-SCHIP-1), and ankyrin (Ank) G. (a and b) Cultured hippocampal neurons (9 DIV) treated either with dimethyl-sulfoxide (DMSO) alone as a control (a) or with 5 μM of 4,5,6, 7-tetrabromobenzotriazole (TBB) (in DMSO) (b) for 24 h were immunostained for IQCJ-SCHIP-1 and AnkG. Scale bar = 20 μm. (c) Quantification of IQCJ-SCHIP-1 and AnkG fluorescent intensity. ***$p < 0.0001$
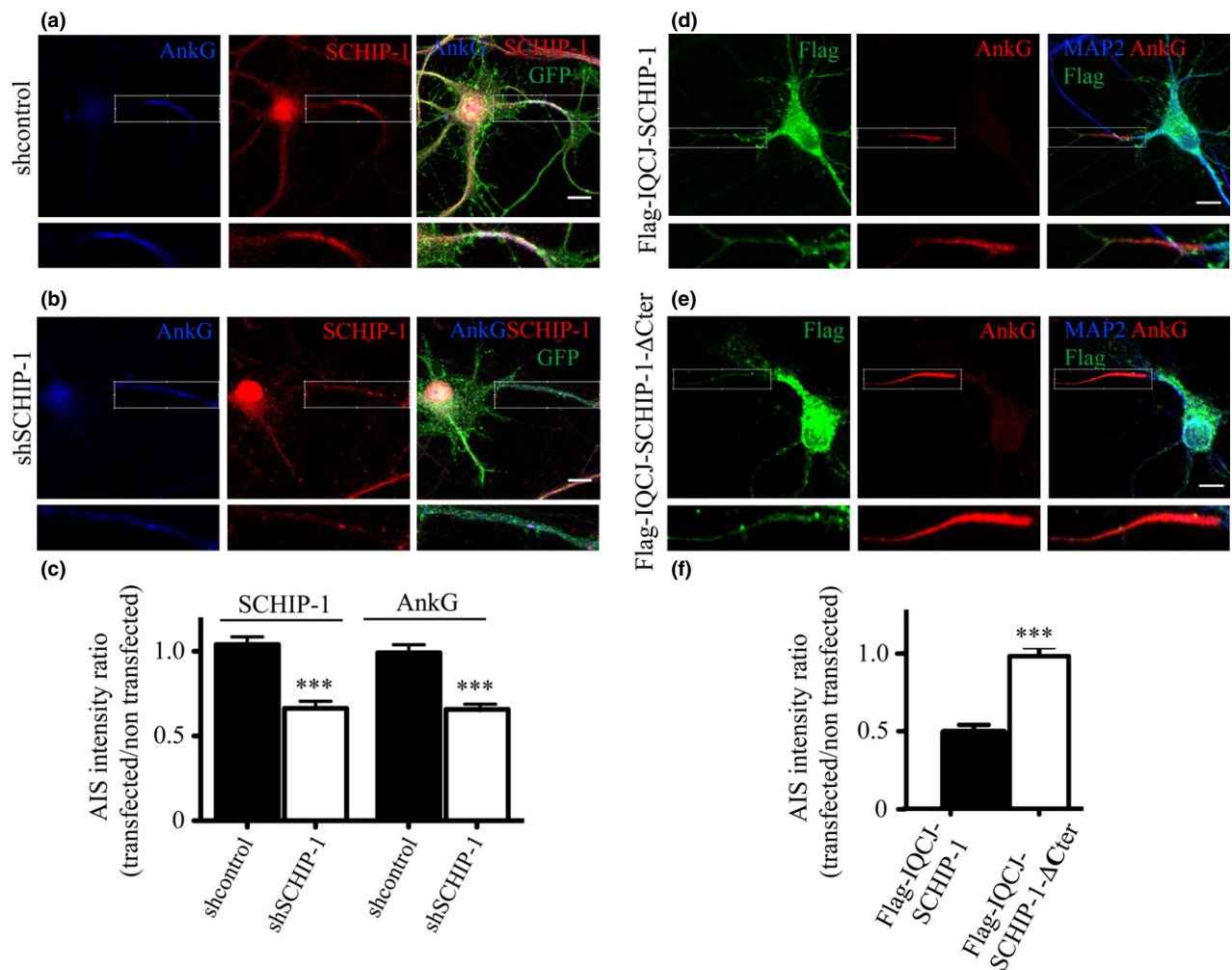
Fig. 5 Effect of IQ motif containing J-Schwannomin-Interacting Protein 1 (IQCJ-SCHIP-1) on ankyrin (Ank) G clustering in the axon initial segment (AIS). (a–c) Effect of IQCJ-SCHIP-1 silencing on IQCJ-SCHIP-1 and AnkG. Neurons transfected with either shluciferase used as a control (a) or shSCHIP-1 (b) were stained with 17141 (red), anti-GFP (green) and anti-AnkG (blue) Abs. Scale bars = 10 μm. (c) The quantification of the AIS intensity ratio in the transfected neuron to that in surrounding non-transfected cells, for IQCJ-SCHIP-1 and AnkG. (d–f) Effect of IQCJ-SCHIP-1 over-expression on AnkG. (d and e) Neurons were transfected with Flag-IQCJ-SCHIP-1 (d) and Flag-IQCJ-SCHIP-1ΔCter (e) were stained with anti-AnkG (red), anti-GFP (green) and anti-MAP2 (blue) Abs. Scale bars = 10 μm. (f) AnkG AIS intensity ratio in the transfected neuron to that in surrounding non-transfected cells. ***$p < 0.0001$

reduced endogenous AnkG clustering at the AIS through its CK2-regulated AnkG-binding site.

Discussion

We previously observed that IQCJ-SCHIP-1 segregated at the AIS of neurons, *in vivo* (Martin *et al.* 2008). In this study, we analyzed the molecular mechanisms involved in IQCJ-SCHIP-1-specific axonal location. We showed that IQCJ-SCHIP-1 accumulated at the AIS of hippocampal neurons in culture and that AnkG depletion reduced its concentration. Both pull-down assays and SPR analysis revealed a direct interaction of nanomolar affinity between AnkG and CK2-phosphorylated IQCJ-SCHIP-1 but not with non-phosphorylated form of the protein. Moreover, we demonstrated that a region of IQCJ-SCHIP-1 including 12 sites phosphorylatable by CK2 was involved in this association. Pharmacological inhibition of CK2 led to a diminution of the IQCJ-SCHIP-1 accumulation at the AIS of cultured neurons. Silencing SCHIP-1 expression reduced AnkG clustering at the AIS. Finally, over-expression of IQCJ-SCHIP-1 in neurons decreased AnkG concentration at the AIS whereas a mutant deleted of the CK2-regulated AnkG interaction site did not. To conclude, our study reveals that CK2-phosphorylation regulates IQJC-SCHIP-1 association with AnkG and consequently its accumulation at the AIS. Our study reveals that CK2-regulated IQJC-SCHIP-1 association with AnkG contributes to AIS maintenance.

CK2 is a Ser and Thr kinase that has pleiotropic effects on a wide range of cellular events. CK2 is thought to be constitutively active and its segregation to specific cell compartments may contribute to its substrate specificity (Montenarh 2010). We previously showed that CK2 was concentrated at the AIS of both cultured neurons and *in vivo*, and that CK2-phosphorylation of the AnkG-binding motif of $Na_v1.2$ and $Na_v1.6$ channels not only enhanced channel affinity to AnkG but also contributed to their accumulation at the AIS (Brechet *et al.* 2008; Brachet *et al.* 2010; Hien *et al.* 2014). Here we report that the interaction between IQJC-SCHIP-1 and AnkG is also regulated by CK2. We observed that the IQ motif of IQCJ-SCHIP-1 was not required for the *in vitro* association between AnkG and IQCJ-SCHIP-1 as CK2-phosphorylated SCHIP-1a, which does not possess this IQ motif, still associated with AnkG with a nanomolar-range affinity.

Our SPR experiments revealed that CK2-phosphorylated IQCJ-SCHIP-1 bound to AnkG and to AnkB with equivalent affinities. This result was not really surprising since these two axonal ankyrins present a high degree of sequence homology (Bennett and Healy 2009). However, IQCJ-SCHIP-1 preferentially accumulates at the AIS (AnkG-positive subdomain), but not in distal axons (AnkB-positive subdomain) of cultured hippocampal neurons. In sciatic nerves, IQCJ-SCHIP-1 proteins co-localized with AnkG in the nodal region of the nodes of Ranvier (Martin *et al.* 2008), but not in the paranodal regions that contain high concentrations of AnkB (Kordeli *et al.* 1990; Ogawa 2006). Thus, altogether these data suggest that IQCJ-SCHIP-1 may preferentially interact *in vivo* with AnkG. One reason for the different results obtained *in vivo* and *in vitro*, may be found in the neuronal conformation and position of the axonal ankyrins. Indeed, AnkG is associated with the plasma membrane *via* a palmitoyl anchor or *via* its interaction with membrane proteins, while AnkB is essentially expressed as an intracellular protein (He *et al.* 2012, 2013). Differences in membrane anchoring and/or in ankyrin conformations may sustain that IQCJ-SCHIP-1 binds preferentially to AnkG. It is also tempting to propose that CK2, which is found enriched in both the AIS and the nodes of Ranvier (Brechet *et al.* 2008), favors only the association between IQCJ-SCHIP-1 and AnkG. This would contribute to IQCJ-SCHIP-1-specific accumulation in only AnkG-positive domains.

Others kinases modulate protein location at the AIS. For example, the cyclin-dependent kinase 2 (cdk2) and cdk5 kinases regulate K_v1 channel targeting through the phosphorylation of their auxiliary subunit $K_v\beta2$ (Vacher *et al.* 2011). Furthermore, cdk5 influences protein distribution in the Ank- enriched AIS-like compartment of γ neurons, in *Drosophila* (Trunova *et al.* 2011). The glycogen-synthase kinase 3 (GSK3) activity was also described to influence both the clustering of AnkG and Na_v and neuronal excitability of cultured neurons (Tapia *et al.* 2012). Interestingly, IQCJ-SCHIP-1 also presents several predicted phosphorylation sites for both cdk2/5 and GSK3 kinases (Xue *et al.* 2008). However, these sites are not located in the CK2-phosphorylatable domain involved in AnkG interaction. Therefore, it is likely that CK2 directs the accumulation of IQCJ-SCHIP-1 at the AIS.

The molecular mechanisms responsible for AnkG retention at the AIS begin to be unraveled. It has been shown that ankyrin B forms an intra–axonal boundary limiting AnkG incorporation into the distal axonal submembranous cytoskeleton and consequently causes its accumulation at the proximal axon (Galiano *et al.* 2012). Moreover, silencing βIV-spectrin or neurofascin in knock-out mice or in cultured neurons did not inhibit AnkG segregation at the AIS, (Hedstrom *et al.* 2008; Le Bras *et al.* 2013), confirming the role of AnkG as the main organizer of the AIS. On the other hand, we ((Brechet *et al.* 2008) and present work) and others (Sanchez-Ponce *et al.* 2011) have shown that the inhibition of CK2 by pharmacological or interference RNA approaches affected AnkG concentration at the AIS, suggesting that AnkG retention at the AIS is also regulated. In the present study, we observed that either depletion of IQCJ-SCHIP-1, or its over-expression, reduced AnkG concentration at the AIS. Moreover, the impact of IQCJ-SCHIP-1 over-expression required the presence of the C-terminal region that carries CK2-regulated AnkG-binding site. Thus, altering the concentration of IQCJ-SCHIP-1 in neurons influences AIS maintenance and this effect depends on CK2-regulated association between IQCJ-SCHIP-1 and AnkG. Altogether, this suggests an interplay between AnkG, IQCJ-SCHIP-1, and CK2 activity: the concentration of AnkG at the AIS would partially depend on its interaction with IQCJ-SCHIP-1, which in turn could be finely controlled by CK2.

References

Bähler M. and Rhoads A. (2002) Calmodulin signaling via the IQ motif. *FEBS Lett.* **513**, 107–113.

Bennett V. and Healy J. (2009) Membrane domains based on ankyrin and spectrin associated with cell-cell interactions. *Cold Spring Harb. Perspect. Biol.* **1**, a003012.

Blasius T. L., Cai D., Jih G. T., Toret C. P. and Verhey K. J. (2007) Two binding partners cooperate to activate the molecular motor Kinesin-1. *J. Cell Biol.* **176**, 11–17.

Bloom L. and Horvitz H. R. (1997) The *Caenorhabditis elegans* gene unc-76 and its human homologs define a new gene family involved in axonal outgrowth and fasciculation. *Proc. Natl Acad. Sci. USA* **94**, 3414–3419.

Brachet A., Leterrier C., Irondelle M., Fache M.-P., Racine V., Sibarita J.-B., Choquet D. and Dargent B. (2010) Ankyrin G restricts ion channel diffusion at the axonal initial segment before the establishment of the diffusion barrier. *J. Cell Biol.* **191**, 383–395.

Brechet A., Fache M.-P., Brachet A., Ferracci G., Baude A., Irondelle M., Pereira S., Leterrier C. and Dargent B. (2008) Protein kinase CK2 contributes to the organization of sodium channels in axonal membranes by regulating their interactions with ankyrin G. *J. Cell Biol.* **183**, 1101–1114.

Catimel B., Layton M., Church N., Ross J., Condron M., Faux M., Simpson R. J., Burgess A. W. and Nice E. C. (2006) In situ phosphorylation of immobilized receptors on biosensor surfaces: application to E-cadherin/β-catenin interactions. *Anal. Biochem.* **357**, 277–288.

Duncan J. S., Gyenis L., Lenehan J., Bretner M., Graves L. M., Haystead T. A. and Litchfield D. W. (2008) An unbiased evaluation of CK2 inhibitors by chemoproteomics characterization of inhibitor effects on CK2 and identification of novel inhibitor targets. *Mol. Cell Proteomics* **7**, 1077–1088.

Fujita T., Maturana A. D., Ikuta J. *et al.* (2007) Axonal guidance protein FEZ1 associates with tubulin and kinesin motor protein to transport mitochondria in neurites of NGF-stimulated PC12 cells. *Biochem. Biophys. Res. Commun.* **361**, 605–610.

Galiano M. R., Jha S., Ho T. S.-Y., Zhang C., Ogawa Y., Chang K.-J., Stankewich M. C., Mohler P. J. and Rasband M. N. (2012) A distal axonal cytoskeleton forms an intra-axonal boundary that controls axon initial segment assembly. *Cell* **149**, 1125–1139.

Garrido J. J. (2003) A targeting motif involved in sodium channel clustering at the axonal initial segment. *Science* **300**, 2091–2094.

Gasser A., Ho T. S.-Y., Cheng X., Chang K.-J., Waxman S. G., Rasband M. N. and Dib-Hajj S. D. (2012) An ankyrinG-binding motif is necessary and sufficient for targeting Nav1.6 sodium channels to axon initial segments and nodes of Ranvier. *J. Neurosci.* **32**, 7232–7243.

Gindhart J. G., Chen J., Faulkner M., Gandhi R., Doerner K., Wisniewski T. and Nandlestadt A. (2003) The kinesin-associated protein UNC-76 is required for axonal transport in the Drosophila nervous system. *Mol. Biol. Cell* **14**, 3356–3365.

Goutebroze L., Brault E., Muchardt C., Camonis J. and Thomas G. (2000) Cloning and characterization of SCHIP-1, a novel protein interacting specifically with spliced isoforms and naturally occurring mutant NF2 proteins. *Mol. Cell. Biol.* **20**, 1699–1712.

He M., Jenkins P. and Bennett V. (2012) Cysteine 70 of ankyrin-G Is S-palmitoylated and is required for function of ankyrin-G in membrane domain assembly. *J. Biol. Chem.* **287**, 43995–44005.

He M., Tseng W.-C. and Bennett V. (2013) A single divergent exon inhibits ankyrin-B association with the plasma membrane. *J. Biol. Chem.* **288**, 14769–14779.

Hedstrom K. L., Xu X., Ogawa Y., Frischknecht R., Seidenbecher C. I., Shrager P. and Rasband M. N. (2007) Neurofascin assembles a specialized extracellular matrix at the axon initial segment. *J. Cell Biol.* **178**, 875–886.

Hedstrom K. L., Ogawa Y. and Rasband M. N. (2008) AnkyrinG is required for maintenance of the axon initial segment and neuronal polarity. *J. Cell Biol.* **183**, 635–640.

Hien Y. E., Montersino A., Castets F., Leterrier C., Filhol O., Vacher H. and Dargent B. (2014) CK2 accumulation at the axon initial segment depends on sodium channel Nav1. *FEBS Lett.* **588**, 3403–3408.

Ikuta J., Maturana A., Fujita T., Okajima T., Tatematsu K., Tanizawa K. and Kuroda S. (2007) Fasciculation and elongation protein zeta-1 (FEZ1) participates in the polarization of hippocampal neuron by controlling the mitochondrial motility. *Biochem. Biophys. Res. Commun.* **353**, 127–132.

Jenkins S. M. (2001) Ankyrin-G coordinates assembly of the spectrin-based membrane skeleton, voltage-gated sodium channels, and L1 CAMs at Purkinje neuron initial segments. *J. Cell Biol.* **155**, 739–746.

Karlsson R., Katsamba P. S., Nordin H., Pol E. and Myszka D. G. (2006) Analyzing a kinetic titration series using affinity biosensors. *Anal. Biochem.* **349**, 136–147.

Komada M. (2002) betaIV-spectrin regulates sodium channel clustering through ankyrin-G at axon initial segments and nodes of Ranvier. *J. Cell Biol.* **156**, 337–348.

Kordeli E., Davis J., Trapp B. and Bennett V. (1990) An isoform of ankyrin is localized at nodes of Ranvier in myelinated axons of central and peripheral nerves. *J. Cell Biol.* **110**, 1341–1352.

Kwaśnicka-Crawford D. A., Carson A. R. and Scherer S. W. (2006) IQCJ–SCHIP1, a novel fusion transcript encoding a calmodulin-binding IQ motif protein. *Biochem. Biophys. Res. Commun.* **350**, 890–899.

Le Bras B., Fréal A., Czarnecki A., Legendre P., Bullier E., Komada M., Brophy P. J., Davenne M. and Couraud F. (2014). In vivo assembly of the axon initial segment in motor neurons. *Brain Struct. Funct.* **219**, 1433–1450.

Lemaillet G. (2003) Identification of a conserved ankyrin-binding motif in the family of sodium channel subunits. *J. Biol. Chem.* **278**, 27333–27339.

Leterrier C. and Dargent B. (2014) No Pasaran! Role of the axon initial segment in the regulation of protein transport and the maintenance of axonal identity. *Semin. Cell Dev. Biol.* **27**, 44–51.

Leterrier C., Vacher H., Fache M.-P., d' Ortoli S. A., Castets F., Autillo-Touati A. and Dargent B. (2011). End-binding proteins EB3 and EB1 link microtubules to ankyrin G in the axon initial segment. *Proc. Natl Acad. Sci. USA* **108**, 8826–8831.

Lois C. (2002) Germline transmission and tissue-specific expression of transgenes delivered by lentiviral vectors. *Science* **295**, 868–872.

Martin P.-M., Carnaud M., del Cano G. G., Irondelle M., Irinopoulou T., Girault J.-A., Dargent B. and Goutebroze L. (2008) Schwannomin-interacting protein-1 isoform IQCJ-SCHIP-1 is a late component of nodes of Ranvier and axon initial segments. *J. Neurosci.* **28**, 6111–6117.

Montenarh M. (2010) Cellular regulators of protein kinase CK2. *Cell Tissue Res.* **342**, 139–146.

Ogawa Y. (2006) Spectrins and ankyrinB constitute a specialized paranodal cytoskeleton. *J. Neurosci.* **26**, 5230–5239.

Palau W. and Di Primo C. (2013) Simulated single-cycle kinetics improves the design of surface plasmon resonance assays. *Talanta* **114**, 211–216.

Pan Z. (2006) A common ankyrin-G-based mechanism retains KCNQ and NaV channels at electrically active domains of the axon. *J. Neurosci.* **26**, 2599–2613.

Sanchez-Ponce D., Muñoz A. and Garrido J. J. (2011) Casein kinase 2 and microtubules control axon initial segment formation. *Mol. Cell Neurosci.* **46**, 222–234.

Sobotzik J.-M., Sie J. M., Politi C., Del Turco D., Bennett V., Deller T. and Schultz C. (2009) AnkyrinG is required to maintain axo-dendritic polarity in vivo. *Proc. Natl Acad. Sci. USA* **106**, 17564–17569.

Tapia M., Del Puerto A., Puime A. *et al.* (2012) GSK3 and β-catenin determines functional expression of sodium channels at the axon initial segment. *Cell. Mol. Life Sci.* **70**, 105–120.

Trunova S., Baek B. and Giniger E. (2011) Cdk5 regulates the size of an axon initial segment-like compartment in mushroom body neurons of the Drosophila central brain. *J. Neurosci.* **31**, 10451–10462.

Vacher H., Yang J.-W., Cerda O., Autillo-Touati A., Dargent B. and Trimmer J. S. (2011) Cdk-mediated phosphorylation of the Kv 2 auxiliary subunit regulates Kv1 channel axonal targeting. *J. Cell Biol.* **192**, 813–824.

Xue Y., Ren J., Gao X., Jin C., Wen L. and Yao X. (2008) GPS 2.0, a tool to predict kinase-specific phosphorylation sites in hierarchy. *Mol. Cell Proteomics* **7**, 1598–1608.

Zhang X. and Bennett V. (1998) Restriction of 480/270-kD ankyrin G to axon proximal segments requires multiple ankyrin G-specific domains. *J. Cell Biol.* **142**, 1571–1581.